Molecular Cell
Article

Structural and Functional Insights into Dom34, a Key Component of No-Go mRNA Decay

Hyung Ho Lee,[1] Youn-Sung Kim,[1] Kyoung Hoon Kim,[1] Inha Heo,[2] Sang Kyu Kim,[1] Olesya Kim,[1] Hye Kyung Kim,[1] Ji Young Yoon,[1] Hyoun Sook Kim,[1] Do Jin Kim,[1] Sang Jae Lee,[1] Hye Jin Yoon,[1] Soon Jong Kim,[3] Byung Gil Lee,[4] Hyun Kyu Song,[4] V. Narry Kim,[2] Chung-Mo Park,[1] and Se Won Suh[1,*]
[1]Department of Chemistry
[2]Department of Biological Sciences
College of Natural Sciences, Seoul National University, Seoul 151-747, Korea
[3]Department of Chemistry, Mokpo National University, Mokpo 534-729, Korea
[4]School of Life Sciences and Biotechnology, Korea University, Seoul 136-701, Korea
*Correspondence: sewonsuh@snu.ac.kr
DOI 10.1016/j.molcel.2007.07.019

SUMMARY

The yeast protein Dom34 is a key component of no-go decay, by which mRNAs with translational stalls are endonucleolytically cleaved and subsequently degraded. However, the identity of the endoribonuclease is unknown. Homologs of Dom34, called Pelota, are broadly conserved in eukaryotes and archaea. To gain insights into the structure and function of Dom34/Pelota, we have determined the structure of Pelota from *Thermoplasma acidophilum* (Ta Pelota) and investigated the ribonuclease activity of Dom34/Pelota. The structure of Ta Pelota is tripartite, and its domain 1 has the RNA-binding Sm fold. We have discovered that Ta Pelota has a ribonuclease activity and that its domain 1 is sufficient for the catalytic activity. We also demonstrate that domain 1 of Dom34 has an endoribonuclease activity against defined RNA substrates containing a stem loop, which supports a direct catalytic role of yeast Dom34 in no-go mRNA decay.

INTRODUCTION

In all organisms, the amount of each mRNA is tightly controlled by the rates of both transcription and decay processes. Large-scale analyses indicate that as many as half of all changes in the amounts of mRNA in some responses can be attributed to altered rates of decay (Garneau et al., 2007). Normal mRNAs undergo decay by three different pathways: the deadenylation-dependent, deadenylation-independent, and endonuclease-mediated decays (Garneau et al., 2007). In addition to turnover of normal mRNAs, mRNAs that undergo abnormal translation in the cytoplasm are targeted for degradation by the mRNA-surveillance pathways (Clement and Lykke-Andersen, 2006; Tollervey, 2006). At least three mRNA-surveillance pathways have been described. The nonsense-mediated decay (NMD) targets mRNAs with premature translation-termination codons (Gonzalez et al., 2001; Losson and Lacroute, 1979; Wilusz et al., 2001), while the nonstop decay (NSD) targets mRNAs lacking termination codons (Frischmeyer et al., 2002; van Hoof et al., 2002; Vasudevan et al., 2002). More recently, a new surveillance pathway, termed no-go decay, was identified in *Saccharomyces cerevisiae* (Doma and Parker, 2006). It targets mRNAs with translation-elongation stalls. In contrast to the former two surveillance pathways, the no-go decay involves endonucleolytic cleavage of the mRNA in the vicinity of the stalled ribosome (Clement and Lykke-Andersen, 2006; Doma and Parker, 2006). This is reminiscent of NMD in *D. melanogaster* (Gatfield and Izaurralde, 2004). Although the full mechanism of no-go decay is not well understood, it appears that mRNA surveillance based on translation elongation rates is a conserved process (Doma and Parker, 2006; Onouchi et al., 2005).

In the no-go decay, stalled ribosomes on an mRNA are detected, and the mRNA is endonucleolytically cleaved near the stall site (Doma and Parker, 2006; Garneau et al., 2007). It was shown that two *S. cerevisiae* proteins, Dom34 and Hbs1 (Hsp70 subfamily B suppressor 1), are required for the initial endonucleolytic cleavage (Doma and Parker, 2006). Each of Dom34 and Hbs1 is related to the translation termination factors eRF1 and eRF3, respectively. However, the endoribonuclease that catalyzes the mRNA cleavage has not been identified, and the roles of Dom34 and Hbs1 in no-go decay have not been characterized at the molecular level. At least three possibilities have been suggested regarding the identity of the endonuclease (Tollervey, 2006). The first is that Dom34 or Hbs1 catalyzes the mRNA cleavage itself, although their sequences apparently do not suggest this. The second is that they could recruit a specific nuclease to the site of cleavage. The third possibility is that interactions with Hbs1 or Dom34 might allow the ribosome itself to cleave the mRNA. An intriguing possibility exists that the no-go decay is not only an mRNA quality control mechanism

but also a means by which the cells could control the abundance of specific mRNAs, thereby regulating gene expression at the translational level (Clement and Lykke-Andersen, 2006; Tollervey, 2006). Consistent with this idea, disruption of the *pelota* gene in mice and fruit flies leads to specific defects in development and cell-cycle progression (Adham et al., 2003; Xi et al., 2005). It has also been suggested that inositol-requiring enzyme-1 (IRE1) may promote translational stalling and cleavage of endoplasmic reticulum-localized mRNAs by no-go decay during the unfolded protein response (Hollien and Weissman, 2006).

In *S. cerevisiae*, deletion of the gene *dom34* causes growth retardation, defective sporulation, and reduced polyribosomes (Davis and Engebrecht, 1998). The yeast Dom34 protein has a strong genetic interaction with the gene *RPS30A*, which encodes the ribosomal protein S30; overexpression of *RPS30A* rescues the growth defects and reduced polyribosomes of Dom34 mutants (Davis and Engebrecht, 1998). It was shown to interact specifically with Hbs1, which is a small GTPase implicated in translational regulation (Carr-Schmid et al., 2002). Dom34 and Hbs1 were proposed to help together directly or indirectly facilitate the expression either of specific mRNAs or under certain cellular conditions (Carr-Schmid et al., 2002). Human and mouse cDNAs encoding the homolog of *S. cerevisiae* Hbs1 were named eukaryotic RF similar (eRFS) (Wallrapp et al., 1998). The N-terminal domains of Hbs1-like proteins and eRF3 differ from each other, whereas their C-terminal domains share sequence similarity (Wallrapp et al., 1998). The mammalian orthologs of *S. cerevisiae* Hbs1 do not carry the eRF3-like activity (Wallrapp et al., 1998).

Genes homologous to the yeast *dom34*, called *pelota*, have been identified in a number of eukaryotes, including human (Shamsadin et al., 2000), mouse (Shamsadin et al., 2002), *Drosophila melanogaster* (Castrillon et al., 1993; Eberhart and Wasserman, 1995), *Caenorhabditis elegans*, and *Arabidopsis thaliana*. Homologous genes are also present in archaebacteria such as *Sulfolobus solfataricus* (Ragan et al., 1996). The eukaryotic Pelota proteins are in general longer than the archaeal members (361–461 residues in eukaryotes versus 332–357 residues in archaea) (Figure 1). As the amino acid sequences of the Dom34/Pelota proteins have been highly conserved during evolution, they constitute an evolutionarily conserved protein family (Adham et al., 2003). The current Pfam classification (Finn et al., 2006; http://www.expasy.org/sprot/) places the Dom34/Pelota proteins into a subfamily of the eukaryotic release factor 1 (eRF1) family, as they are presumed to consist of three eRF1-like domains (eRF1_1, eRF1_2, and eRF1_3).

Translational control of eukaryotic gene expression (Pickering and Willis, 2005) plays an essential role in the differentiation and development of animal cells (Edwards et al., 2001), as it provides an important checkpoint in the pathways for cell growth and differentiation (Gray and Wickens, 1998; Willis, 1999). Biochemical and genetic studies indicate that eukaryotic Dom34/Pelota plays an important role in cell division, differentiation of germline stem cells, and stem cell self-renewal by controlling the expression of specific genes at the translational level. However, the precise mechanism of translation regulation by Dom34/Pelota has not yet been revealed. *D. melanogaster* Pelota was proposed to act at the level of protein translation, replacing the yeast Dom34 protein (Eberhart and Wasserman, 1995). In *D. melanogaster*, the *pelota* (*pelo*) gene is required for the meiotic cell division during the G_2/M transition (Eberhart and Wasserman, 1995). It is required prior to the first meiotic division for spindle formation and nuclear envelope breakdown during spermatogenesis (Eberhart and Wasserman, 1995). It is also required for normal eye patterning and for mitotic cell divisions in the ovary (Eberhart and Wasserman, 1995). The meiotic defect in *pelota* mutants may be a complex result of a protein translation defect, as suggested in yeast by the ribosomal protein S30 being a multicopy suppressor and by an altered polyribosome profile in Dom34 mutants rescued by expression of *RPS30A* (Davis and Engebrecht, 1998). In mice, a *pelo* knockout causes early embryonic lethality with defects in cell division and proliferation (Adham et al., 2003). A new biological role of *D. melanogaster* Pelota in controlling stem cell self-renewal has been revealed (Xi et al., 2005). It was shown to function as an intrinsic factor to control germline stem cell self-renewal by repressing a Bam-independent differentiation pathway, possibly through regulating translation (Xi et al., 2005). As Dom34/Pelota is highly conserved from fruit flies to mammals, there is a possibility that Dom34/Pelota may also be involved in the regulation of adult stem cell self-renewal in mammals, including humans (Xi et al., 2005).

To unravel the functional role of Dom34/Pelota in the no-go mRNA-surveillance pathway and translation regulation, structural and functional studies on Dom34/Pelota are required. Here we report the crystal structure of a representative member of the Dom34/Pelota family, the cell division protein Pelota from *Thermoplasma acidophilum* (Ta Pelota). Ta Pelota shows sequence identity of 26%, 22%, and 21% with Dom34/Pelota from human, *D. melanogaster*, and *S. cerevisiae*, respectively. It has a tripartite architecture, with the structural similarity to eRF1 being limited to domains 2 and 3 only. Our structure reveals that domain 1 of Dom34/Pelota is unrelated to domain 1 of eRF1 and that it resembles the RNA binding Sm and Lsm (Sm-like) proteins (Kambach et al., 1999; Khusial et al., 2005; Mura et al., 2001; Wilusz and Wilusz, 2005). We have discovered that Ta Pelota has a ribonuclease activity and that its domain 1 is sufficient for the catalytic activity. We have also characterized *S. cerevisiae* Dom34 functionally by investigating a possible ribonuclease activity using defined RNA substrates with a stable stem loop. We demonstrate that *S. cerevisiae* Dom34 has an endoribonuclease activity that could explain the endonucleolytic cleavage of the stalled mRNA in no-go decay. These findings have significant implications for the function of Dom34/Pelota in no-go mRNA decay and translation regulation of gene expression in eukaryotes.

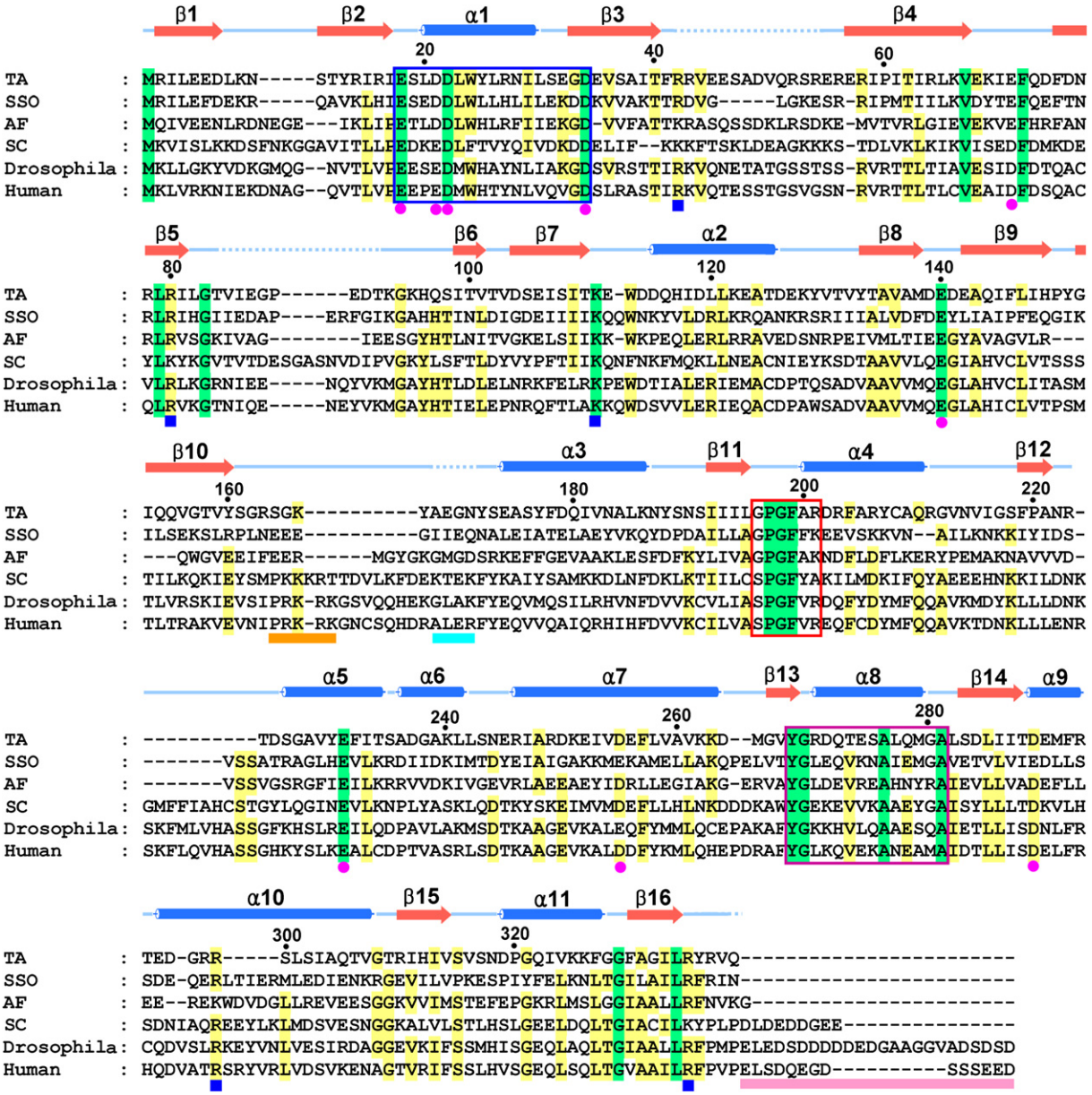

Figure 1. Alignment of Dom34/Pelota Amino Acid Sequences

TA, *T. acidophilum* (SWISS-PROT accession code Q9HJ74); SSO, *S. solfataricus* (P96026); AF, *A. fulgidus* (O29421); SC, *S. cerevisiae* (P33309); *Drosophila*, *D. melanogaster* (P48612); Human, *Homo sapiens* (Q9BRX2). Strictly conserved residues and semiconserved residues are colored in green and yellow, respectively. Cylinders above the sequences denote α helices and arrows β strands. Blue dotted lines represent disordered residues. Three signature sequence motifs are enclosed in colored boxes: motif I (residues 18–34) in blue, motif II (196–201) in red, and motif III (268–281) in purple, respectively. This figure was drawn with ClustalX (Thompson et al., 1997) and GeneDoc (http://www.psc.edu/biomed/genedoc). Orange, cyan, and pink bars below the sequences denote the putative nuclear localization signal in eukaryotic Pelotas, the position corresponding to the GGQ motif of human eRF1, and the acidic C-terminal tail in eukaryotic Pelotas, respectively. The conserved negatively charged residues and positively charged residues are indicated by pink circles and blue squares below the sequences.

RESULTS AND DISCUSSION

Overall Structure

We have determined the crystal structure of Ta Pelota by the multiwavelength anomalous diffraction (MAD) method (Table 1). The model accounts for 312 residues of the 339-residue polypeptide chain of Ta Pelota and 17 water molecules in each asymmetric unit. Twenty-six residues in three regions of the polypeptide chain (Arg42–Arg54, Thr84–Thr92, and Ala168–Asn171) and the C-terminal residue (Gln339), as well as the eight-residue affinity tag (LEHHHHHH) fused at the C terminus, are missing from

Table 1. Data Collection, Phasing, and Refinement Statistics

	Native	SeMet 1			SeMet 2		
Data Collection							
Space group	$P4_32_12$	$P4_32_12$			$P4_32_12$		
Unit cell dimensions							
a = *b* (Å)	98.06	98.47			97.85		
c (Å)	150.10	150.04			150.11		
		Peak	Edge	Remote	Peak	Edge	Remote
Wavelength (Å)	1.00000	0.97945	0.97965	0.97178	0.97945	0.97965	0.97178
Resolution (Å)[a]	50–2.90 (3.04–2.90)	50–3.10 (3.21–3.10)	50–3.10 (3.21–3.10)	50–3.10 (3.21–3.10)	50–3.10 (3.21–3.10)	50–3.10 (3.21–3.10)	50–3.35 (3.47–3.35)
I/σ_I [a]	11.1 (3.4)	9.0 (2.8)	9.1 (2.8)	9.1 (2.6)	8.9 (2.8)	8.8 (2.9)	8.2 (2.0)
R_{merge} (%)[a,b]	9.5 (46.5)	9.2 (25.9)	8.0 (25.2)	6.6 (34.9)	9.3 (22.5)	8.6 (26.0)	6.6 (50.6)
Completeness (%)[a]	98.5 (90.1)	98.8 (97.8)	98.7 (97.1)	98.7 (97.9)	98.2 (97.1)	98.2 (96.5)	98.6 (97.9)
Redundancy[a]	19.1 (13.0)	7.9 (8.0)	7.9 (8.0)	7.9 (8.0)	8.0 (8.1)	8.0 (8.1)	8.0 (8.1)
Figure of merit[c]		0.70 for 30–3.1 Å					
Refinement			Model Quality				
Resolution (Å)	15–2.90		Rmsd				
Number of reflections	15,309		Bond lengths (Å)		0.0086		
R_{work}/R_{free} (%)[d]	21.4/26.2		Bond angles (°)		1.53		
Number of nonhydrogen atoms/ mean B factor (Å^2)			Ramachandran plot (%)				
Protein	2495/67.3		Most favorable		87.1		
Water	17/64.3		Allowed		12.2		
			Generously allowed		0.7		
			Disallowed		0.0		

[a] Numbers in parentheses correspond to the highest-resolution shell.
[b] $R_{merge} = \Sigma_h\Sigma_i|I(h)_i - < I(h) > |/\Sigma_h\Sigma_i I(h)_i$, where $I(h)$ is the intensity of reflection h, Σ_h is the sum over all reflections, and Σ_i is the sum over i measurements of reflection h.
[c] Figure of merit = $|\sum P(\alpha)e^{i\alpha}/\sum P(\alpha)|$, where $P(\alpha)$ is the phase probability distribution and α is the phase.
[d] R_{work} and $R_{free} = \sum||F_o|-|F_c||/\sum|F_o|$ for the working set and test set (10%) of reflections.

the model, since they have no electron density. The model has been refined to crystallographic R_{work} and R_{free} values of 21.4% and 26.2%, respectively, for 15–2.9 Å data without a sigma cutoff (Table 1).

Ta Pelota is tripartite; it is organized into three domains of similar size (Figure 2). The three domains are arranged in a cloverleaf-like fashion (Figure 2), with a single polypeptide chain connecting two adjacent domains. Domain 1 (residues 1–129) contains a helix (α1) and seven antiparallel β strands that are arranged in the order β1↓-β2↑-β7↓-β3↑-β4↓-β5↑-β6↓. The latter five β strands form a distorted β barrel, which, together with helix α1, represents a highly divergent version of the Sm fold (Khusial et al., 2005). The architecture of domain 1 has no resemblance to domain 1 of eRF1 (Song et al., 2000). Helix α2 serves as the linker between domain 1 and domain 2 (Figure 2). Domain 2 (residues 130–242) has a five-stranded mixed β sheet packed on one side by a pair of helices (α3 and α4) and on the other side by another pair of helices (α5 and α6). The strands of the β sheet are arranged in the order β12↑-β11↑-β8↑-β9↓-β10↑. Domain 3 (residues 243–339) forms a mixed four-stranded β sheet, packed on one side by two α helices (α7 and α11) and on the other side by three α helices (α8, α9, and α10). The strands of the β sheets are arranged in the order β13↑-β16↓-β14↑-β15↑.

Oligomeric State of Ta Pelota in Solution

In the crystal, Ta Pelota forms a dimeric unit by association of two monomers that are related by crystallographic twofold symmetry. The solvent accessible surface area buried at the interface between the two monomers in this dimeric

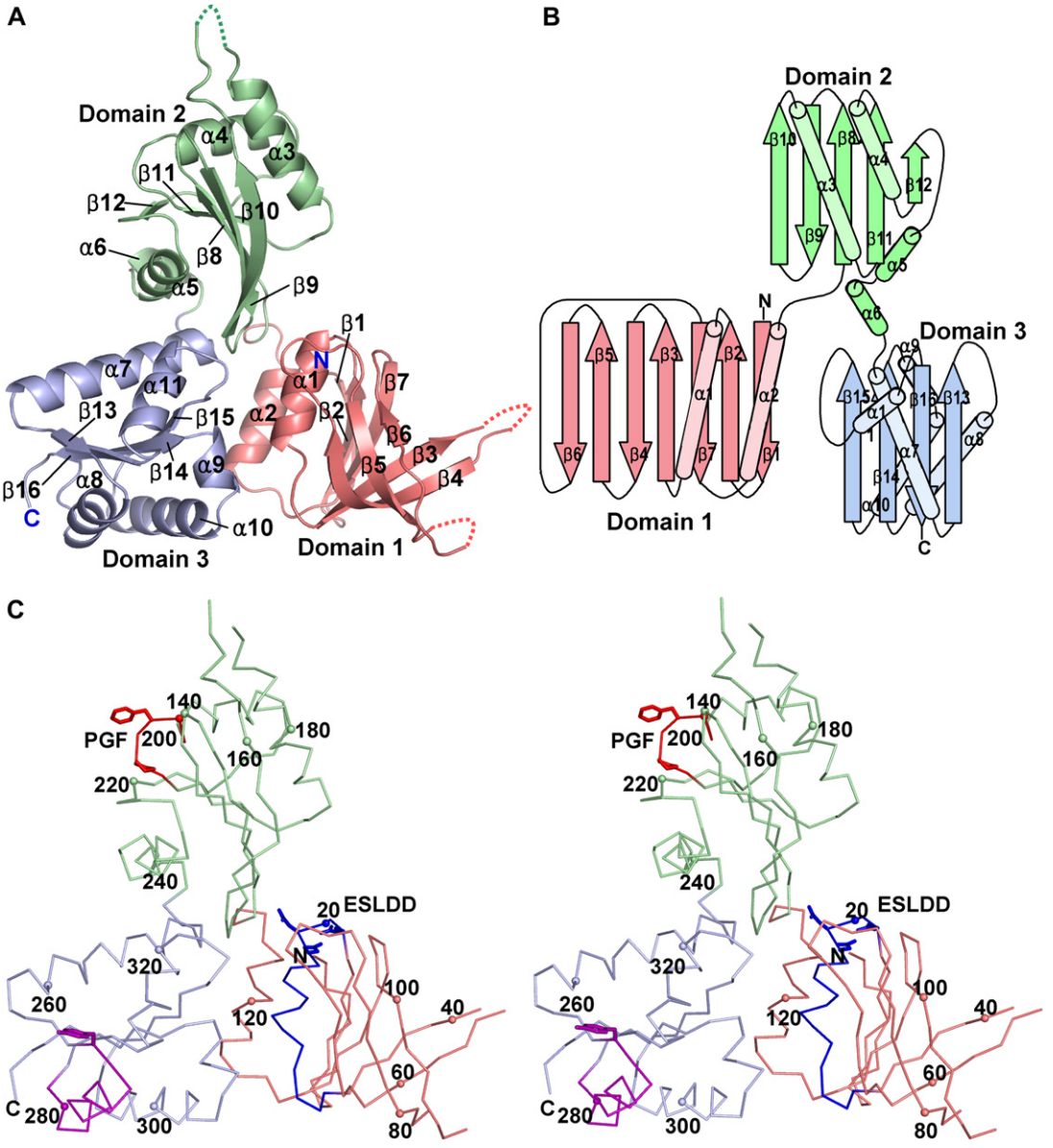

Figure 2. Overall Structure of Ta Pelota

(A) Ribbon diagram. Each domain is colored in different colors. Secondary structure elements were defined by PyMOL (DeLano, 2002). Three disordered regions are represented in dotted lines. All the figures except Figures 1 and 2B are drawn with PyMOL.

(B) Topology diagram. α helices are shown as cylinders and β strands as arrows.

(C) Stereo Cα trace. Each domain is colored in different colors. Every 20th residue is marked by a dot and labeled. Three signature sequence motifs are highlighted in colored lines: motif I [(**E**)xx(D/E)(**D**)(L/M)(WF)xxxxhhxxx(**D**)] at positions 18–34 in blue, motif II [(G/S)**PGF**$x_{1\sim2}$(K/R)] at positions 196–201 in red, and motif III [**YG**xxxxxx(**A**)xxxx(**A**)] at positions 268–281 in purple, respectively.

unit is ~1000 Å^2 (~6% of the monomer surface area), with 41% of the atoms in this interface being polar (Protein-Protein Interaction Server at http://www.biochem.ucl.ac.uk/bsm/PP/server/). This finding raised the possibility that Ta Pelota may be present as dimers in solution. To accurately assess the oligomeric state of Ta Pelota in solution, we carried out sedimentation equilibrium centrifugation (see Figure S1 in the Supplemental Data available with this article online). Figure S1 shows the data and fits for monomer and dimer at the ultracentrifugal speeds of 14,000 and 20,000 rpm, respectively. The global root-mean-square (rms) errors for the monomeric fit analysis at 14,000 and 20,000 rpm were 4.39×10^{-3} and 5.15×10^{-3}, respectively, which demonstrates the goodness of the fit. In contrast, trials to fit to a dimeric model showed systematic deviations from the data, as shown in the residual plots with rms values of 2.27×10^{-2} and 6.57×10^{-2}, respectively. The actual fits are shown in the lower

panels, and plots of distributions of the residuals are shown in the upper panels (Figure S1). These data clearly indicate that Ta Pelota exists as monomers in solution, and the observed dimerization of Ta Pelota in the crystal is not physiologically relevant.

Structural Similarity Search

A search for overall structural similarities with the full-length Ta Pelota using the DALI program (Holm and Sander, 1993) failed to reveal any significant matches. For more detailed searches, we performed structural similarity searches with each domain. Domain 1 alone (Met1–Tyr129) of Ta Pelota showed very low structural similarities (Z score < 4.5). The highest Z score is obtained with the *Pyrobaculum aerophilum* Sm protein (Mura et al., 2001) (PDB code 1I8F; an rmsd of 2.7 Å for 60 equivalent Cα positions in residues 10–80, a Z score of 4.3, and a sequence identity of 15%). Compared to the previous structures of the Sm fold (Khusial et al., 2005), Ta Pelota domain 1 has two additional β strands (β1 and β2) in front of the starting helix (α1) of the Sm fold and an extra helix (α2) at the C terminus (Figure 3A). The additional helix α2 may be regarded as part of an extended linker between domain 1 and domain 2. It covers one side of the additional β strands β1 and β2 that lie next to the last strand of the β barrel of the Sm fold. Conceivably, the structural resemblance of Pelota domain 1 to Sm/Lsm proteins could imply functional relatedness. Sm proteins and Lsm proteins form hexameric or heptameric rings of ~70 Å in diameter (Khusial et al., 2005) (Figure 3B). In the lumen of the ring, the repeating motifs bind the single-stranded RNA (Khusial et al., 2005). However, unlike Sm and Lsm proteins, domain 1 of Pelota is fused to eRF1-like domains 2 and 3, and our structure shows that domain 1 of Pelota does not form an oligomeric ring. Two loops of the Sm fold proteins provide the RNA binding site or RNA-binding knuckles (Khusial et al., 2005): one loop between the second and third strands, and the other loop between the fourth and the fifth strands (Khusial et al., 2005). The first knuckle has a conserved Asn, and the second knuckle has Arg (Figure 3A). The first knuckle corresponds to the loop between β4 and β5 in the Pelota structure, and the second knuckle corresponds to the loop between β5 and β6. Compared to other structures of the Sm fold, the fourth strand of Ta Pelota is much shorter, and Ta Pelota does not carry the conserved Asn or Arg residue in the corresponding regions (Figures 1 and 3A). It appears that the structural resemblance alone between Pelota domain 1 and Sm proteins is not sufficient to suggest a functional mimic.

Both domain 2 (residues 130–242) and domain 3 (residues 243–338) of Ta Pelota match well with their counterparts from human eRF1 (Figures 3C and 4). The highest Z score for domain 2 is obtained with domain 2 of human eRF1 (PDB code 1DT9; an rmsd of 2.5 Å for 105 equivalent Cα positions, residues 143–275, a Z score of 11.6, and a sequence identity of 7%). The highest Z score for domain 3 is obtained with domain 3 of the human Pelota (cgi-17) (unpublished deposition; PDB code 1X52; an rmsd of 1.6 Å for 94 equivalent Cα positions in residues 14–115, a Z score of 13.7, and a sequence identity of 27%). The second highest Z score is obtained with domain 3 of human eRF1 (PDB code 1DT9; an rmsd of 2.3 Å for 94 equivalent Cα positions in residues 276–415, a Z score of 11.8, and a sequence identity of 26%). The relative orientation between domain 2 and domain 3 in Ta Pelota is much different from that between corresponding domains in eRF1 (Figure 4C), implying conformational flexibility.

Conceivably, sharing of two structurally similar domains in the C-terminal two-thirds of the polypeptide chains of Dom34/Pelota and eRF1 (Figure 3C) may be suggestive of functional relatedness. However, all members of the Dom34/Pelota protein family lack the universal GGQ sequence motif (in domain 2) of class 1 release factors, which triggers the hydrolytic activity of the peptidyltransferase center of the ribosome from both prokaryotes and eukaryotes (Song et al., 2000). This absence makes it likely that the functional correspondence between Dom34/Pelota and eRF1 is indirect and subtle, if there is any. Interestingly, a strictly conserved tripeptide Pro-Gly-Phe (PGF) motif is present in domain 2 of the Dom34/Pelota proteins (Figures 1 and 2C). The structural dissimilarity between domains 1 and the presence of different sequence motifs in domains 2 suggest that it would be more appropriate to categorize Dom34/Pelota and eRF1 into two distinct protein families, although they are apparently evolutionarily related to each other in their C-terminal domains.

Sequence Motifs of Dom34/Pelota

Sequence alignment of the Dom34/Pelota family members reveals three highly conserved sequence motifs (Figure 1). Motif I in domain 1 [**E**xx(D/E)**D**(L/M)(W/F)xxxxhhxxx**D**] encompasses Glu18–Asp34 of Ta Pelota (boxed in blue in Figure 1). Motif II in domain 2 [(G/S)**PGF**$x_{1\sim2}$(K/R)] covers Gly196–Arg201 of Ta Pelota (boxed in red in Figure 1), while motif III in domain 3 [**YG**xxxxxx**A**xxxx**A**] covers Tyr268–Ala281 of Ta Pelota (boxed in purple in Figure 1). "h" is a hydrophobic residue, "x" stands for any amino acid, and the residues that are strictly conserved in Figure 1 are in boldface.

Motif I of Dom34/Pelota is rich in acidic residues, which is reminiscent of the metal ion binding motif of the enzymes that utilize a two-metal-ion-catalyzed phosphoryl-transfer mechanism (Steitz and Steitz, 1993), although it does not show any homology to known sequence motifs in the active site of such enzymes. This feature, coupled with the observed structural resemblance of domain 1 to the RNA-binding Sm proteins, hints the possibility that Dom34/Pelota could possess a ribonuclease activity. Indeed, we demonstrate in this study that Ta Pelota (either full-length or domain 1 alone) has such a catalytic activity and that the conserved acidic residues of sequence motif I are important for the ribonuclease activity (Figure 6). Asp34 makes a salt bridge with Lys111, which is strictly conserved.

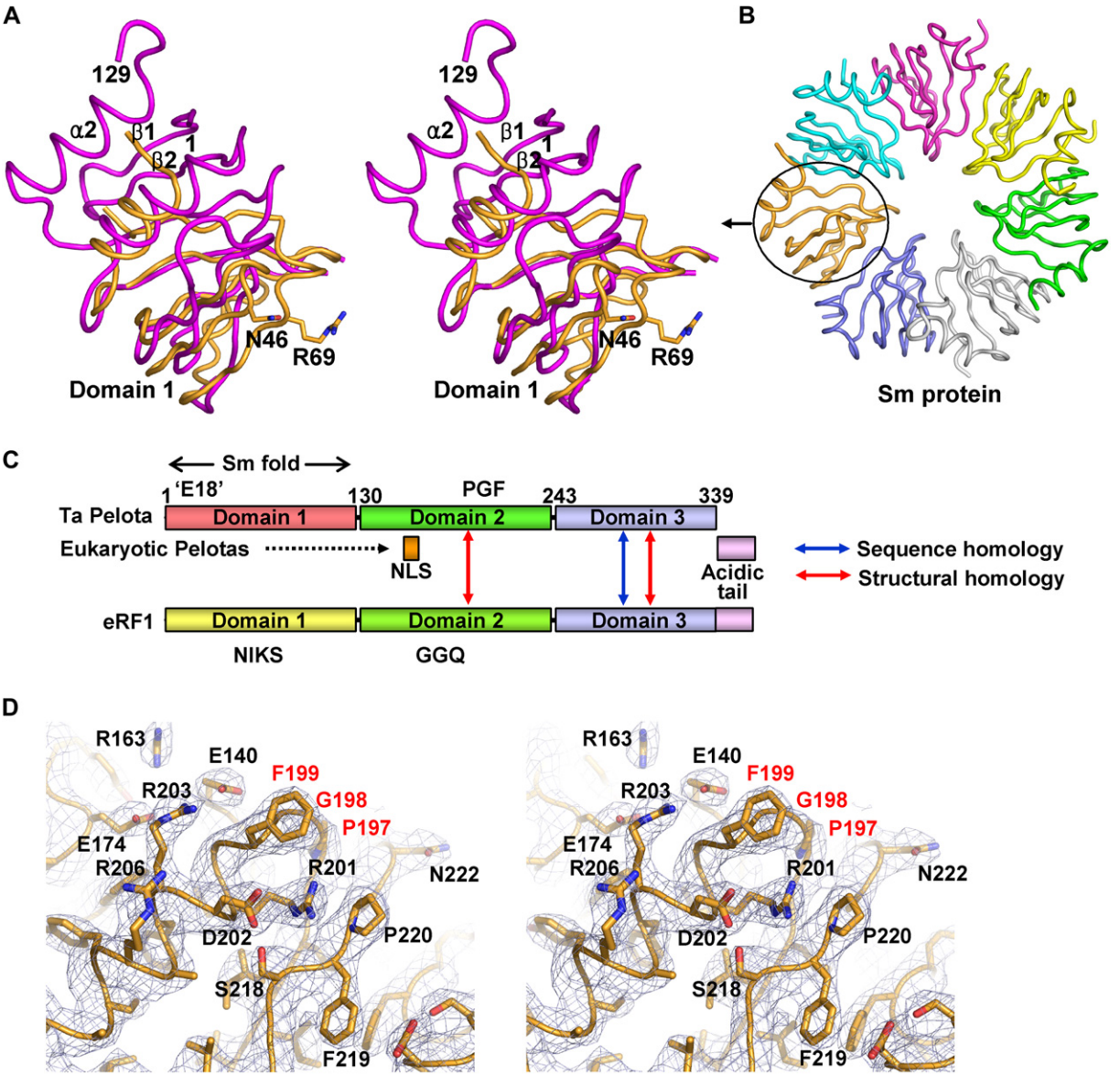

Figure 3. Structural Comparison of Ta Pelota and the Sm Protein from *P. aerophilum*

(A) Superposition of domain 1 of Ta Pelota (magenta tube) and the *P. aerophilum* Sm protein (orange tube) (PDB code 1I8F; Mura et al. [2001]). The conserved Asn46 and Arg69 of the *P. aerophilum* Sm protein, termed RNA-binding knuckles (Khusial et al., 2005), are shown.

(B) Heptamer structure of the *P. aerophilum* Sm protein.

(C) Schematic diagram comparing domain structures of Ta Pelota and eRF1.

(D) Stereo $2F_o - F_c$ electron density map around the Pro197-Gly198-Phe199 sequence of Ta Pelota.

A tripeptide motif, Pro-Xxx-Thr or Ser-Pro-Phe, that is present in domain 1 of bacterial class 1 release factors, RF1 and RF2, respectively, confers stop codon specificity in a hybrid RF1/RF2 protein (Ito et al., 2000). These tripeptides have been hypothesized to interact directly with the second and third codon nucleotides (Ito et al., 2000). In human eRF1, the NIKS motif in domain 1 was proposed to recognize the stop codons (Song et al., 2000). There is no such conserved tripeptide or tetrapeptide motif in domain 1 of Dom34/Pelota. The absence of the NIKS motif in domain 1 of Dom34/Pelota is consistent with the role of the yeast Dom34 in recognizing mRNAs with stalls in translation elongation (Doma and Parker, 2006). Our structural and functional data (discussed below) allow us to propose that the eukaryotic Dom34/Pelota proteins recognize a stem-loop structure of the stalled mRNA and their domain 1 functions as the endoribonuclease (Figure 6). Furthermore, domain 1 of Ta Pelota bears no

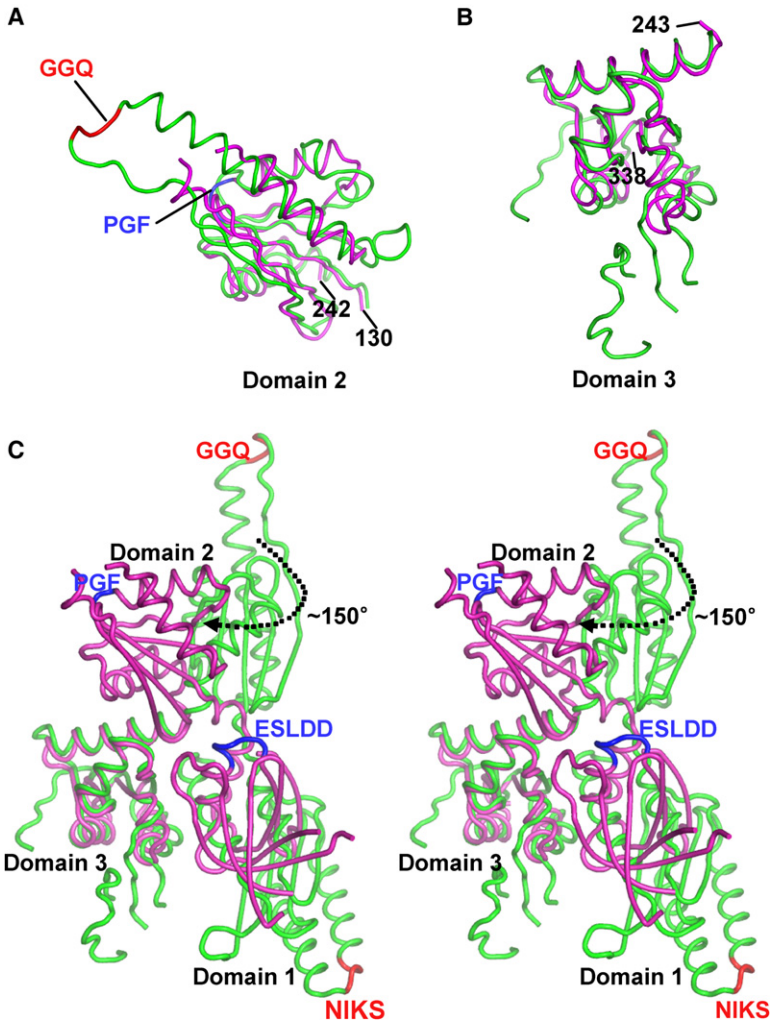

Figure 4. Structural Comparison of Ta Pelota and Human eRF1

(A) Superposition of Ta Pelota domain 2 (magenta tube) and the corresponding domain of human eRF1 (green tube).

(B) Superposition of Ta Pelota domain 3 (magenta tube) and the corresponding domain of human eRF1 (green tube).

(C) Superposition of Ta Pelota (magenta tube) and human eRF1 (green tube). Domain 3 of human eRF1 is superposed with that of Ta Pelota. The PGF sequence (in motif II) and ESLDD sequence (part of motif I) of Ta Pelota are colored in blue. The GGQ and NIKS motifs of human eRF1 are colored in red.

structural resemblance to the corresponding domains of human eRF1 (Song et al., 2000) and the *E. coli* RF2 (Vestergaard et al., 2001). It is worth mentioning that there exists archaeal RF1 (aRF1) that has both the NIKS motif in domain 1 and the GGQ motif in domain 2.

Motif II of Dom34/Pelota contains the strictly conserved tripeptide sequence PGF. The conservation suggests a universal and essential role of the PGF sequence in the Dom34/Pelota function. The PGF motif of Ta Pelota (Pro197-Gly198-Phe199) is located on the protein surface at a turn connecting the β strand β11 with the N terminus of the helix α4 in domain 2 (Figure 2C). The side chain of Phe199 points toward the bulk solvent (Figure 3D). It is well suited to interact with a potential binding partner, either a nucleic acid or a polypeptide chain, if the role of the PGF motif is specific recognition. It was proposed that Gln185 of the GGQ motif participates in the coordination of the water molecule at the peptidyltransferase center of the ribosome that is responsible for hydrolyzing the peptidyl-tRNA ester bond (Song et al., 2000). By functional relatedness, it is conceivable that the PGF motif in domain 2 of Dom34/Pelota may be involved in an interaction with the ribosome and at a site distinct from the peptidyltransferase center. The class 1 release factors (eRF1, bacterial RF1 and RF2) have the universal GGQ motif at an exposed tip of domain 2 (Figure 4C) (Song et al., 2000). Within the human eRF1 structure, the GGQ motif is located on a turn connecting an extended region of a β strand with the N terminus of the helix α5, and it occurs within a context rich in arginine and lysine residues (Song et al., 2000). In contrast, the surrounding region around the PGF motif is not rich in arginine and lysine residues. The equivalent position of GGQ in Dom34/Pelota is highly variable in sequence and is disordered in the structure of Ta Pelota (Figures 1 and 2). Motif III of Dom34/Pelota contains a strictly conserved tyrosine residue (Tyr268 in Ta Pelota). This tyrosine residue is located near the protein surface in domain 3 of Ta Pelota at the C terminus of β13, which resides between helices α7 and α8 (Figure 2C).

Ribonuclease Activity of Dom34/Pelota

Ta Pelota showed a ribonuclease activity against a total RNA substrate (Figure 6A). When the substrate RNA was incubated in the reaction buffer in the absence of Ta Pelota, it was not degraded (lane 1 in Figures 6A and 6B). Therefore, the observed ribonuclease activity is clearly an inherent property of Ta Pelota but is not due to contaminating nucleases in the reaction buffer. The ribonuclease activity of Ta Pelota was strongly inhibited by EDTA or vanadyl ribonucleoside complexes (Figure 6A, lanes 6 and 7). The high concentration of EDTA required for inhibition of Ta Pelota may be attributed to the possibility that the total RNA sample used as the substrate contains a high concentration of divalent metal ions such as Mg^{2+}. Domain 1 alone of Ta Pelota showed a ribonuclease activity comparable to the full-length (Figure 6A, lane 8), whereas domain 3 showed no activity (Figure 6A, lane 10). We could not check the activity of domain 2 due to poor solubility. This suggests that domain 1 of Ta Pelota is sufficient for the ribonuclease activity. The ribonuclease activity of domain 1 was also strongly inhibited by vanadyl ribonucleoside complexes (Figure 6A, lane 9). Domain 1 of the yeast Dom34 protein shows a strong ribonuclease activity against the total RNA, whereas its domain 3 does not (Figure 6A, lanes 11 and 12).

In order to pinpoint the key residues essential for the ribonuclease activity of Ta Pelota, we have prepared four single mutants (E18A, D21A, D22A, and E231A) and three double mutants (E18A/D21A, E18A/D22A, and D21A/D22A). The ribonuclease activity of Ta Pelota was largely diminished by the mutations E18A, E18A/D21A, E18A/D22A, and D21A/D22A (Figure 6B, lanes 3, 6, 7, and 8, respectively). In comparison, two other single mutants (D21A and D22A) retained the ribonuclease activity (Figure 6B, lanes 4 and 5). The ribonuclease activity of the E231A mutant was also diminished (Figure 6B, lane 9). Glu231 is highly conserved and is located at the interface between domains 2 and 3 on helix α5 (Figure 5B). These results suggest that conserved acidic residues (Glu18, Asp21, and Asp22) of sequence motif I and possibly Glu231 play important roles in the ribonuclease activity of Ta Pelota. The side chains of Glu18, Asp21, and Asp22 are exposed to the solvent in the Ta Pelota structure (Figure 5A). On one side of the Ta Pelota structure, a continuous positively charged surface patch is formed in domain 1 adjacent to the negatively charged surface around the conserved Glu18, Asp21, and Asp22 (Figure 5B). These two surface regions together could constitute the active site of the ribonuclease, with the positively charged surface playing a role in recognizing the RNA substrate. Site-directed mutagenesis experiments, together with deletion mutations, clearly demonstrate that the ribonuclease activity of Ta Pelota is not due to some copurifying and contaminating *E. coli* nucleases. In order to check if yeast Dom34 might possess the ribonuclease activity like Ta Pelota, we have expressed Dom34 and Hbs1 separately in *E. coli* and purified each of them as well as the Dom34/Hbs1 complex (Figure 6C). Both the Dom34/Hbs1 complex and Hbs1 itself were stable, whereas Dom34 alone aggregated rapidly after purification. The ribonuclease activity of the full-length Dom34 was weaker than its domain 1, which we ascribe to its tendency for aggregation, and Hbs1 alone did not show a strong ribonuclease activity (Figure 6B, lanes 10 and 11). The Dom34/Hbs1 complex exhibited a strong ribonuclease activity (Figure 6B, lane 12), which hints at the possibility of the direct catalytic role of the yeast Dom34 protein in no-go mRNA decay (Doma and Parker, 2006).

To demonstrate the endoribonuclease activity of *S. cerevisiae* Dom34, we synthesized defined RNA substrates containing a stable stem loop (34 base pair) by in vitro transcription (188-mer substrate 1 and 168-mer substrate 2 in Figure 6D) and examined the cleavage products (Figures 6E–6G). The two RNA substrates differ in the length of the 5′ side single-stranded region. Due to the rapid aggregation of the full-length Dom34 after purification, we used $Dom34_{1-138}$ (corresponding to domain 1) in these experiments. In a ribonuclease assay with the RNA substrate 1 that was internally labeled with [α-^{32}P]CTP, we could identify four major cleavage product bands (labeled as P1 (~82-mer), P2 (~63-mer), P3 (~33-mer), and P4 (~32-mer) in Figure 6E, lane 3) as well as minor bands corresponding to the partially digested products (Figure 6E, lane 3, marked with asterisks). With the RNA substrate 2 that was internally labeled with [α-^{32}P]CTP, we could also identify four major cleavage product bands (labeled as P1′ (~62-mer), P2 (~63-mer), P3 (~33-mer), and P4 (~32-mer) in Figure 6E, lane 4) as well as minor bands corresponding to the partially digested products (Figure 6E, lane 4, marked with asterisks). The estimated sizes of the fragments are subject to an error by several bases. From the size of these cleavage product bands, we can envision four possible cleavage sites (Figure 6D). The P1 and P1′ product bands are derived by cleavage at the C1 site from the 5′ side of substrates 1 and 2, respectively, and this interpretation is supported by the digestion pattern of the 5′ end-labeled substrates 1 and 2 (Figure 6F, lanes 1–4, 7, and 8). The P2 product band is derived from the 3′ side of either substrate 1 or 2 by cleavage at the C2 site, and this interpretation is supported by the digestion pattern of the 3′ end labeled substrates 1 and 2 (Figure 6G). The C1 and C2 cleavage sites reside on the double-stranded region of the RNA substrates and are approximately one helical turn separated from the junction between the single-stranded region and the double-stranded region of the RNA substrate. The P3 product band is most likely to be derived from the stem loop upon cleavages at the C1 and C3 sites, while the P4 product band is most likely to be derived from the stem loop upon cleavages at the C2 and C4 sites (Figure 6D). This interpretation is supported by the absence of the P3 and P4 product bands in the digestion pattern of either the 5′ end-labeled substrates (Figure 6F, lanes 1–4, 7 and 8) or the 3′ end-labeled substrates (Figure 6G). Our observation that $Dom34_{1-138}$ does not cleave the single-stranded region of the two RNA substrates but cleaves the

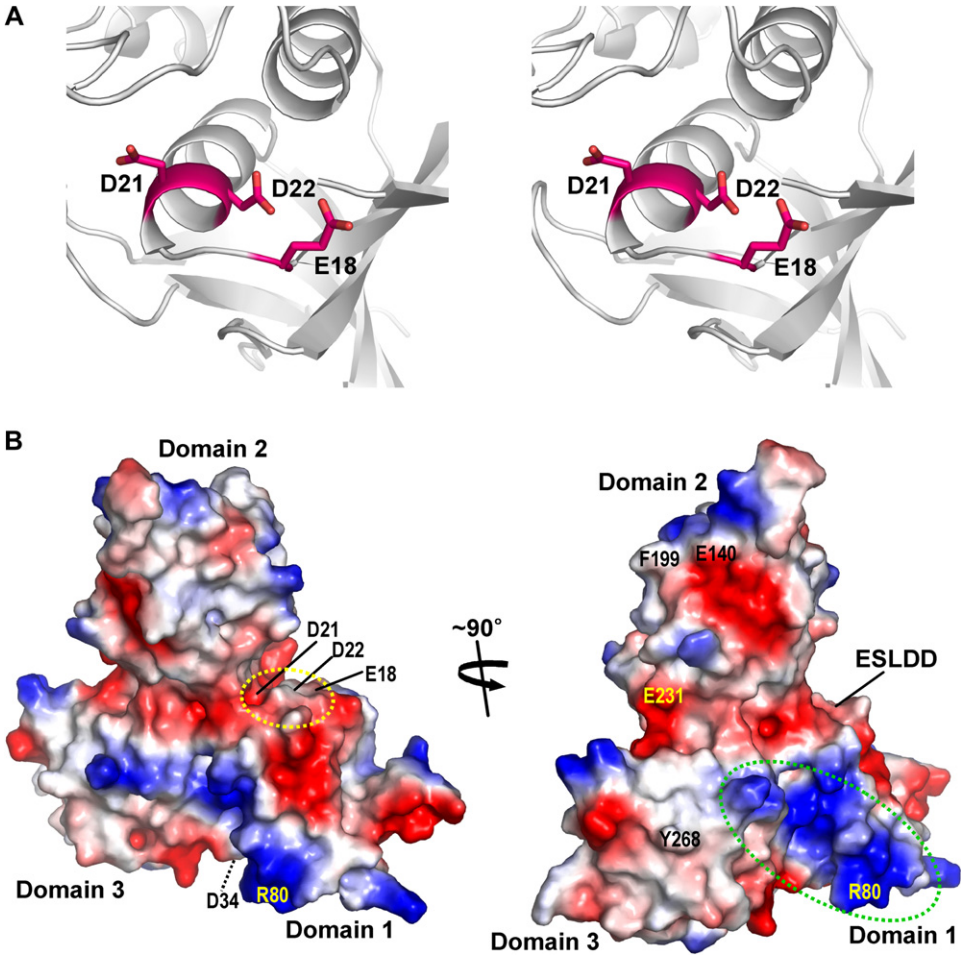

Figure 5. Putative Active Site and Surface View of Ta Pelota

(A) Stereo ribbon diagram around the putative active site. Three conserved acidic residues in motif I are shown.

(B) Two different views of the electrostatic potential at the molecular surface of Ta Pelota (blue, positive; red, negative). They are roughly 90° apart. The location of conserved acidic residues in motif I is indicated by the yellow dotted ellipse. The green dotted ellipse on the right panel indicates the positively charged surface patch next to sequence motif I.

double-stranded region at defined sites suggests that the endoribonuclease activity of $Dom34_{1-138}$ may be largely structure specific.

When we cleaved the 5′ end-labeled substrate 1 by $Dom34_{1-138}$, the intensity of the P1 cleavage product (~82-mer) increased with the reaction time, but its position remained unchanged (Figure 6F, lanes 2–4). When we cleaved the 3′ end-labeled substrate 2 by $Dom34_{1-138}$, the intensity of the P2 cleavage product (~63-mer) increased with the reaction time, but its position remained unchanged (Figure 6G, lanes 2–4). These results clearly indicate that Dom34 (domain 1) has a ribonuclease activity of the endo type but no detectable 5′→3′ or 3′→5′ exoribonuclease activities. The endoribonuclease activity of $Dom34_{1-138}$ was completely inhibited by EDTA or vanadyl ribonucleoside complexes (Figure 6F, lanes 5 and 6). The inferred cleavage sites within the stem loop are in good agreement with the proposed multiple cleavages at or near the ribosomal stall site in vivo (Doma and Parker, 2006), although trimming by exoribonucleases from the original cleavage site(s) could have complicated the in vivo cleavage pattern. Our in vitro data on the endoribonuclease activity of $Dom34_{1-138}$ are consistent with a direct catalytic role of Dom34 in no-go mRNA decay.

Conclusions

The current classification of the Dom34/Pelota proteins into a subfamily of the eRF1 family needs to be reassessed in view of our present structural and functional studies, which show that domain 1 of Dom34/Pelota bears the Sm fold and is structurally unrelated to domain 1 of eRF1. We have demonstrated the endoribonuclease activity of the *S. cerevisiae* Dom34 protein, thus providing a line of experimental evidence that the yeast

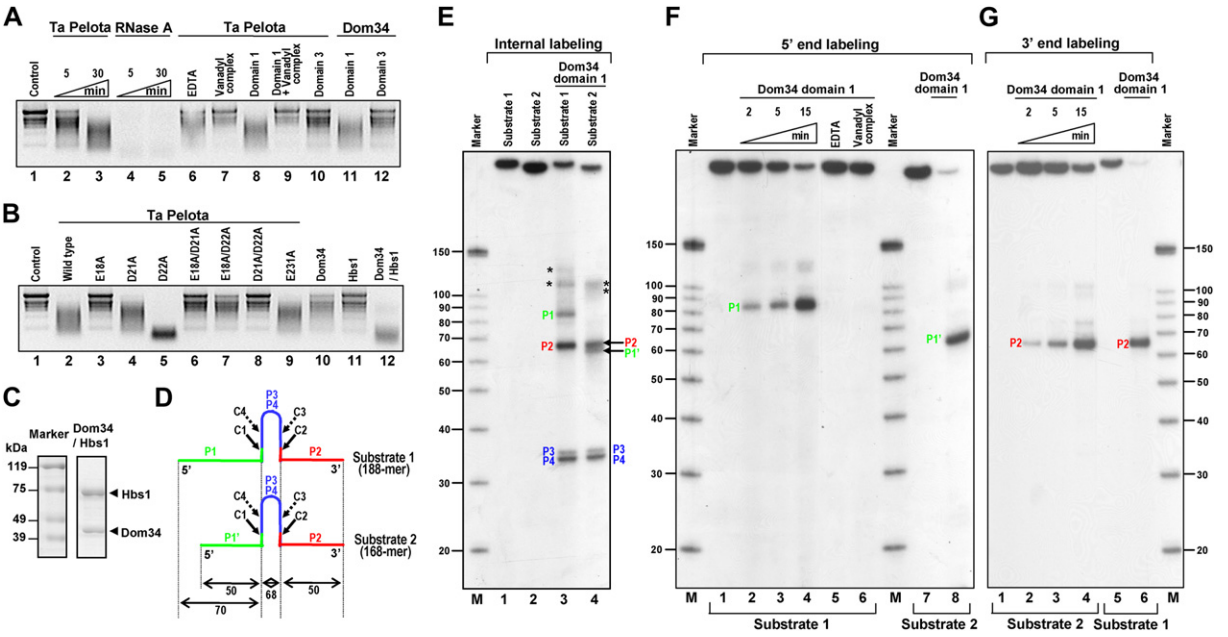

Figure 6. Ribonuclease Activity of Ta Pelota with a Total RNA Substrate and Endoribonuclease Activity of Dom34 with Defined RNA Substrates Containing a Stem Loop

(A) Ribonuclease activity of Ta Pelota (full length and domain 1), bovine pancreatic ribonuclease A, and Dom34 (domain 1) with a total RNA substrate. Lane 1, total RNA + buffer C (10 mM Tris-HCl [pH 7.4], and 100 mM NaCl); lanes 2 and 3, RNA + Ta Pelota (full length); lanes 4 and 5, RNA + bovine pancreatic ribonuclease A; lane 6, RNA + Ta Pelota (full length) + 12.5 mM EDTA; lane 7, RNA + Ta Pelota (full length) + 10 mM vanadyl ribonucleoside complexes; lane 8, RNA + Ta Pelota (domain 1); lane 9, RNA + Ta Pelota (domain 1) + 10 mM vanadyl ribonucleoside complexes; lane 10, RNA + Ta Pelota (domain 3); lane 11, RNA + Dom34 (domain 1); lane 12, RNA + Dom34 (domain 3). All reactions except lanes 2 and 4 (for 5 min) were carried out in buffer C at 40°C for 30 min and were separated by 1.2% (w/v) denaturing formaldehyde-agarose gel electrophoresis.

(B) Ribonuclease activity of the full-length Ta Pelota (wild-type and point mutants) and the Dom34/Hbs1 complex with a total RNA substrate. Lane 1, total RNA + buffer C; lane 2, RNA + Ta Pelota wild-type; lane 3, RNA + E18A mutant; lane 4, RNA + D21A mutant; lane 5, RNA + D22A mutant; lane 6, RNA + E18A/D21A mutant; lane 7, RNA + E18A/D22A mutant; lane 8, RNA + D21A/D22A mutant; lane 9, RNA + E231A mutant; lane 10, RNA + Dom34; lane 11, RNA + Hbs1; lane 12, RNA + Dom34/Hbs1 complex. All reactions were carried out in buffer C at 40°C for 30 min and were separated by 1.2% (w/v) denaturing formaldehyde-agarose gel electrophoresis.

(C) Sodium dodecyl sulfate-polyacrylamide gel electrophoresis of the purified Dom34/Hbs1 complex along with the size marker proteins.

(D) Schematic diagram of the proposed cleavage sites on defined RNA substrates 1 and 2 (188-mer and 168-mer, respectively). The locations of C3 and C4 cleavage sites within the stem loop are less precisely defined and thus are indicated by dashed arrows. Numbers of bases are indicated below the substrates.

(E) Analysis of the cleavage products from internally labeled substrates. Lane M, RNA size marker (Decade markers, Ambion); lane 1, substrate 1 only; lane 2, substrate 2 only; lane 3, substrate 1 + $Dom34_{1–138}$; lane 4, substrate 2 + $Dom34_{1–138}$. Minor bands in lane 3 marked with asterisks are ~125-mer corresponding to substrate 1 minus P2 and ~106-mer corresponding to substrate 1 minus P1. Minor bands in lane 4 marked with asterisks are ~106-mer corresponding to substrate 2 minus P1′ and ~105-mer corresponding to substrate 2 minus P2.

(F) Time course experiment and inhibition of the endoribonuclease activity of $Dom34_{1–138}$ with 5′ end-labeled substrates. Lane M, RNA size marker (Decade markers, Ambion); lane 1, substrate 1 only; lanes 2–4, substrate 1 + $Dom34_{1–138}$ (2, 5, and 15 min, respectively); lane 5, substrate 1 + $Dom34_{1–138}$ + 5 mM EDTA; lane 6, substrate 1 + $Dom34_{1–138}$ + 5 mM vanadyl ribonucleoside complexes; lane 7, substrate 2 only; lane 8, substrate 2 + $Dom34_{1–138}$.

(G) Time course experiment of the ribonuclease assay with 3′ end-labeled RNA substrates. Lane 1, substrate 2 only; lanes 2–4, substrate 2 + $Dom34_{1–138}$ (2, 5, and 15 min, respectively); lane 5, substrate 1 only; lane 6, substrate 1 + $Dom34_{1–138}$; lane M, RNA size marker (Decade markers, Ambion). The amount of the RNA sample loaded into lane 1 is ~60% of those loaded into lanes 2–4. The amount of the RNA sample loaded into lane 5 is ~60% of that loaded into lane 6.

Dom34/Hbs1 complex itself could be the unidentified endoribonuclease in no-go mRNA decay. To our knowledge, domain 1 of Dom34/Pelota is the first case of an Sm fold protein showing the ribonuclease activity, with its motif I representing a signature sequence for a new family of ribonuclease. The ribonuclease activity of Dom34/Pelota could be important for translational regulation of gene expression in eukaryotes—for example, in controlling stem cell self-renewal in fruit flies. Our work, together with the previous results from others, establishes Dom34/Pelota as a unique translation factor with a ribonuclease activity that is distantly related to eRF1 but is distinct from it. We propose from our functional data that Dom34 constitutes the catalytic machinery responsible for the endoribonucleolytic cleavage of the stalled mRNA in no-go decay.

EXPERIMENTAL PROCEDURES

Protein Expression, Purification, and Mutagenesis

Cloning, expression, purification, and mutagenesis of Ta Pelota are given in the Supplemental Data.

The genes encoding the yeast Dom34 and Hbs1 were cloned into the expression vector pET-21a(+) (Novagen) individually. Dom34 was fused with a hexahistidine-containing tag at its C terminus and purified essentially as Ta Pelota, while Hbs1 was expressed either with a hexahistidine-containing tag at its N terminus or in the intact form. Hbs1 with an N-terminal fusion tag was purified by three chromatographic steps involving the nickel-nitrilotriacetic acid-agarose column, the heparin column, and the HiLoad XK-16 Superdex 200 prep-grade column essentially as Ta Pelota. The Dom34/Hbs1 complex was prepared by mixing the *E. coli* cells, each of which expressed Dom34 (fused with a C-terminal tag) and Hbs1 (no tag), respectively, and purified by two chromatographic steps involving the nickel-nitrilotriacetic acid-agarose column and the HiLoad XK-16 Superdex 200 prep-grade column.

Dom34 domain 1 (residues 1–138, with a C-terminal fusion tag) and domain 3 (residues 265–386, with both N- and C-terminal tags) were expressed in soluble form in *E. coli*, whereas domain 2 (residues 139–264, with a C-terminal fusion tag) was expressed as insoluble. Dom34 domain 1 and domain 3 were purified by the same procedure as Ta Pelota, except that the heparin column was not used for domain 3. Point mutants of $Dom34_{1–138}$ (E23A, E23K, E26A, E23K/E26A, E23K/E26K, E23K/D27A, E23K/D27K, E26A/D27A, and E26K/D27K), with a C-terminal fusion tag, were expressed as insoluble in *E. coli*. Single and double mutants were prepared using the QuikChange Site-Directed Mutagenesis Kit (Stratagene) following the manufacturer's instructions. The mutations were confirmed by DNA sequencing.

Ribonuclease Assay with Defined RNA Substrates

Ribonuclease activity was assayed with defined RNA substrates, which were prepared by in vitro transcription with T7 RNA polymerase (Promega) from a pGEM-7Zf(+) plasmid (Promega) that contained a synthetic DNA. A 166-mer oligonucleotide with the following sequence was used as the template for PCR: 5′-TATAT CAAATCGTTCGTTGAGCGAGTTCTCAAAAATGAACAAATGTCGACG ATATCCCGTGGAGGGGCGCGTGGTGGCGGCTGCAGCCGCCACC ACGCGCCCCTCCACGGGATATCGGATCCTTCAACTTCCCTGAGCT CGAAGACGCCAAAAACATAAAGAAAGG-3′. The underlined bases form a 34 base pair stem loop. The stem-loop sequence is identical to one inserted into PGK1 mRNA (Doma and Parker, 2006), except for the first base and the last base. The template sequence was amplified using the following forward and reverse primers that contained the AatII and XhoI cleavage sites (in boldface): 5′-GCG**GACGTC**TATAT CAAATCGTTCGTTGAGCGAGTTC-3′ and 5′-CCGCCG**CTCGAG**CCT TTCTTTATGTTTTTGGCGTCTTCGA-3′. The amplified DNA was cut with AatII/XhoI and was inserted into the AatII/XhoI-digested plasmid pGEM-7Zf(+). When the pGEM-7Zf(+)plasmid containing the synthetic DNA is linearized by XhoI cleavage, in vitro transcription produces the following sequence: 5′-GGGCGAAUUGGGCCCGACGUCUAUAUCA AAUCGUUCGUUGAGCGAGUUCUCAAAAAUGAACAAAUGUCGACG AUAUCCCGUGGAGGGGCGCGUGGUGGCGGCUGCAGCCGCCACC ACGCGCCCCUCCACGGGAUAUCGGATCCUUCAACUUCCCUGAGC UCGAAGACGCCAAAAACAUAAAGAAAGGC-3′ (188-mer RNA; substrate 1).

Substrate 2 was prepared by inserting a linker sequence into the AatII/SalI-digested plasmid pGEM-7Zf(+) containing substrate 1. The linker sequence is prepared by annealing two sequences: 5′-CGCGAGTTCTCAAAAATGAACAAATG-3′ and 5′-TCGACATTTGTT CATTTTTGAGAACTCGCGACG T-3′. Then the pGEM-7Zf(+)plasmid containing substrate 2 was linearized by XhoI, and in vitro transcription produces the following sequence: 5′-GGGCGAAUUGGGCCCGACGU CGCGAGUUCUCAAAAAUGAACAAAUGUCGACGAUAUCCCGUGGA GGGGCGCGUGGUGGCGGCUGCAGCCGCCACCACGCGCCCCUC CACGGGAUAUCGGATCCUUCAACUUCCCUGAGCUCGAAGACGC CAAAAACAUAAAGAAAGGC-3′ (168-mer RNA; substrate 2). The sequences were confirmed by DNA sequencing. The RNA substrates were internally labeled with [α-^{32}P]CTP by in vitro transcription. 5′ end-labeled substrates were prepared by phosphorylating at the 5′ end using T4 polynucleotide kinase (TaKaRa) and [γ-^{32}P]ATP. For 3′ end-labeled substrates, RNAs were labeled with ^{32}P-pCp using T4 RNA ligase (TaKaRa) at 4°C overnight. After the labeling reaction, the RNA substrates were phenol extracted and precipitated with ethanol. The RNA substrates were briefly (~1 min) heated to 100°C and were placed in ice for more than 10 min to prevent the formation of dimers due to the presence of a stable stem loop.

The reaction buffer contained 10 mM Tris-HCl (pH 7.4), 100 mM NaCl, 20 units of RNase inhibitor, and 2 mM $MgCl_2$. The protein (10 ng of $Dom34_{1–138}$) was added to 10 μl of the reaction mixture followed by the addition of the internally or end-labeled RNA substrate. The molar ratio of RNA to protein was approximately 10. The reaction mixture was incubated for up to 30 min at 37°C. Digested RNAs were phenol extracted from the reaction mixture and precipitated with ethanol. They were analyzed on 7 M urea/12.5% polyacrylamide denaturing gels. RNA size markers (Decade markers, Ambion) labeled at the 5′ end were used. After electrophoresis, the gel was exposed to an X-ray film.

Supplemental Data

Supplemental Data include Supplemental Experimental Procedures, Supplemental References, and one figure and can be found with this article online at http://www.molecule.org/cgi/content/full/27/6/938/DC1/.

ACKNOWLEDGMENTS

We thank the beamline staffs for assistance during data collection (BL-4A and BL-6B of Pohang Light Source, Korea, and BL-5A of Photon Factory, Japan). This work was supported by the Korea Ministry of Science and Technology (New Drug Target Discovery Research Grant to S.W.S.).

Received: July 10, 2006
Revised: May 4, 2007
Accepted: July 19, 2007
Published: September 20, 2007

REFERENCES

Adham, I.M., Sallam, M.A., Steding, G., Korabiowska, M., Brinck, U., Hoyer-Fender, S., Oh, C., and Engel, W. (2003). Disruption of the pelota gene causes early embryonic lethality and defects in cell cycle progression. Mol. Cell. Biol. *23*, 1470–1476.

Carr-Schmid, A., Pfund, C., Craig, E.A., and Kinzy, T.G. (2002). Novel G-protein complex whose requirement is linked to the translational status of the cell. Mol. Cell. Biol. *22*, 2564–2574.

Castrillon, D.H., Gonczy, P., Alexander, S., Rawson, R., Eberhart, C.G., Viswanathan, S., DiNardo, S., and Wasserman, S.A. (1993). Toward a molecular genetic analysis of spermatogenesis in *Drosophila melanogaster*: characterization of male-sterile mutants generated by single P element mutagenesis. Genetics *135*, 489–505.

Clement, S.L., and Lykke-Andersen, J. (2006). No mercy for messages that mess with the ribosome. Nat. Struct. Mol. Biol. *13*, 299–301.

Davis, L., and Engebrecht, J. (1998). Yeast dom34 mutants are defective in multiple developmental pathways and exhibit decreased levels of polyribosomes. Genetics *149*, 45–56.

DeLano, W.L. (2002). The PyMOL Molecular Graphics System (http://www.pymol.org).

Doma, M.K., and Parker, R. (2006). Endonucleolytic cleavage of eukaryotic mRNAs with stalls in translation elongation. Nature *440*, 561–564.

Eberhart, C.G., and Wasserman, S.A. (1995). The pelota locus encodes a protein required for meiotic cell division: an analysis of G2/M arrest in *Drosophila* spermatogenesis. Development *121*, 3477–3486.

Edwards, T.A., Pyle, S.E., Wharton, R.P., and Aggarwal, A.K. (2001). Structure of Pumilio reveals similarity between RNA and peptide binding motifs. Cell *105*, 281–289.

Finn, R.D., Mistry, J., Schuster-Bockler, B., Griffiths-Jones, S., Hollich, V., Lassmann, T., Moxon, S., Marshall, M., Khanna, A., Durbin, R., et al. (2006). Pfam: clans, web tools and services. Nucleic Acids Res. *34*, D247–D251.

Frischmeyer, P.A., van Hoof, A., O'Donnell, K., Guerrerio, A.L., Parker, R., and Dietz, H.C. (2002). An mRNA surveillance mechanism that eliminates transcripts lacking termination codons. Science *295*, 2258–2261.

Garneau, N.L., Wilusz, J., and Wilusz, C.J. (2007). The highways and byways of mRNA decay. Nat. Rev. Mol. Cell Biol. *8*, 113–126.

Gatfield, D., and Izaurralde, E. (2004). Nonsense-mediated messenger RNA decay is initiated by endonucleolytic cleavage in *Drosophila*. Nature *429*, 575–578.

Gonzalez, C.I., Bhattacharya, A., Wang, W., and Peltz, S.W. (2001). Nonsense-mediated mRNA decay in *Saccharomyces cerevisiae*. Gene *274*, 15–25.

Gray, N.K., and Wickens, M. (1998). Control of translation initiation in animals. Annu. Rev. Cell Dev. Biol. *14*, 399–458.

Hollien, J., and Weissman, J.S. (2006). Decay of endoplasmic reticulum-localized mRNAs during the unfolded protein response. Science *313*, 104–107.

Holm, L., and Sander, C. (1993). Protein structure comparison by alignment of distance matrices. J. Mol. Biol. *233*, 123–138.

Ito, K., Uno, M., and Nakamura, Y. (2000). A tripeptide 'anticodon' deciphers stop codons in messenger RNA. Nature *403*, 680–684.

Kambach, C., Walke, S., Young, R., Avis, J.M., de la Fortelle, E., Raker, V.A., Luhrmann, R., Li, J., and Nagai, K. (1999). Crystal structures of two Sm protein complexes and their implications for the assembly of the spliceosomal snRNPs. Cell *96*, 375–387.

Khusial, P., Plaag, R., and Zieve, G.W. (2005). LSm proteins form heptameric rings that bind to RNA via repeating motifs. Trends Biochem. Sci. *30*, 522–528.

Losson, R., and Lacroute, F. (1979). Interference of nonsense mutations with eukaryotic messenger RNA stability. Proc. Natl. Acad. Sci. USA *76*, 5134–5137.

Mura, C., Cascio, D., Sawaya, M.R., and Eisenberg, D.S. (2001). The crystal structure of a heptameric archaeal Sm protein: implications for the eukaryotic snRNP core. Proc. Natl. Acad. Sci. USA *98*, 5532–5537.

Onouchi, H., Nagami, Y., Haraguchi, Y., Nakamoto, M., Nishimura, Y., Sakurai, R., Nagao, N., Kawasaki, D., Kadokura, Y., and Naito, S. (2005). Nascent peptide-mediated translation elongation arrest coupled with mRNA degradation in the *CGS1* gene of *Arabidopsis*. Genes Dev. *19*, 1799–1810.

Pickering, B.M., and Willis, A.E. (2005). The implications of structured 5′ untranslated regions on translation and disease. Semin. Cell Dev. Biol. *16*, 39–47.

Ragan, M.A., Logsdon, J.M., Jr., Sensen, C.W., Charlebois, R.L., and Doolittle, W.F. (1996). An archaebacterial homolog of pelota, a meiotic cell division protein in eukaryotes. FEMS Microbiol. Lett. *144*, 151–155.

Shamsadin, R., Adham, I.M., von Beust, G., and Engel, W. (2000). Molecular cloning, expression and chromosome location of the human pelota gene PELO. Cytogenet. Cell Genet. *90*, 75–78.

Shamsadin, R., Adham, I.M., and Engel, W. (2002). Mouse pelota gene (Pelo): cDNA cloning, genomic structure, and chromosomal localization. Cytogenet. Genome Res. *97*, 95–99.

Song, H., Mugnier, P., Das, A.K., Webb, H.M., Evans, D.R., Tuite, M.F., Hemmings, B.A., and Barford, D. (2000). The crystal structure of human eukaryotic release factor eRF1—mechanism of stop codon recognition and peptidyl-tRNA hydrolysis. Cell *100*, 311–321.

Steitz, T.A., and Steitz, J.A. (1993). A general two-metal-ion mechanism for catalytic RNA. Proc. Natl. Acad. Sci. USA *90*, 6498–6502.

Thompson, J.D., Gibson, T.J., Plewniak, F., Jeanmougin, F., and Higgins, D.G. (1997). The CLUSTAL_X windows interface: flexible strategies for multiple sequence alignment aided by quality analysis tools. Nucleic Acids Res. *25*, 4876–4882.

Tollervey, D. (2006). RNA lost in translation. Nature *440*, 425–426.

van Hoof, A., Frischmeyer, P.A., Dietz, H.C., and Parker, R. (2002). Exosome-mediated recognition and degradation of mRNAs lacking a termination codon. Science *295*, 2262–2264.

Vasudevan, S., Peltz, S.W., and Wilusz, C.J. (2002). Non-stop decay—a new mRNA surveillance pathway. Bioessays *24*, 785–788.

Vestergaard, B., Van, L.B., Andersen, G.R., Nyborg, J., Buckingham, R.H., and Kjeldgaard, M. (2001). Bacterial polypeptide release factor RF2 is structurally distinct from eukaryotic eRF1. Mol. Cell *8*, 1375–1382.

Wallrapp, C., Verrier, S.B., Zhouravleva, G., Philippe, H., Philippe, M., Gress, T.M., and Jean-Jean, O. (1998). The product of the mammalian orthologue of the *Saccharomyces cerevisiae* HBS1 gene is phylogenetically related to eukaryotic release factor 3 (eRF3) but does not carry eRF3-like activity. FEBS Lett. *440*, 387–392.

Willis, A.E. (1999). Translational control of growth factor and proto-oncogene expression. Int. J. Biochem. Cell Biol. *31*, 73–86.

Wilusz, C.J., and Wilusz, J. (2005). Eukaryotic Lsm proteins: lessons from bacteria. Nat. Struct. Mol. Biol. *12*, 1031–1036.

Wilusz, C.J., Wormington, M., and Peltz, S.W. (2001). The cap-to-tail guide to mRNA turnover. Nat. Rev. Mol. Cell Biol. *2*, 237–246.

Xi, R., Doan, C., Liu, D., and Xie, T. (2005). Pelota controls self-renewal of germline stem cells by repressing a Bam-independent differentiation pathway. Development *132*, 5365–5374.

Accession Numbers

Coordinates have been deposited in the Research Collaboratory for Structural Bioinformatics (RCSB) Protein Data Bank (PDB) with the PDB code of 2QI2.